Numerical simulations of sunspots

G.J.J. Botha[1], A.M. Rucklidge[1] and N.E. Hurlburt[2]

[1]Department of Applied Mathematics, University of Leeds, Leeds LS2 9JT, UK
email: gert@maths.leeds.ac.uk; A.M.Rucklidge@leeds.ac.uk

[2]Lockheed Martin Solar and Astrophysics Laboratory, Organization L9-41, Building 252, Palo Alto, CA 94304, USA
email: hurlburt@lmsal.com

Abstract. The origin, structure and evolution of sunspots are investigated using a numerical model. The compressible MHD equations are solved with physical parameter values that approximate the top layer of the solar convection zone. A three dimensional (3D) numerical code is used to solve the set of equations in cylindrical geometry, with the numerical domain in the form of a wedge. The linear evolution of the 3D solution is studied by perturbing an axisymmetric solution in the azimuthal direction. Steady and oscillating linear modes are obtained.

Keywords. (magnetohydrodynamics:) MHD, Sun: magnetic fields, sunspots

---

1. Introduction

On the visible surface of the sun, magnetic flux is pushed to the boundaries of granules and supergranules where they (possibly) grow in field strength to becomes pores. These pores have characteristic flow patterns around them (Sobotka *et al.* 1999) and may have rudimentary penumbral structures (Sankarasubramanian & Rimmele 2003). Pores may grow into sunspots, which can have lifetimes of up to several weeks. High-resolution observations have shown that sunspots possess intricate magnetic structures and flow patterns (Langhans *et al.* 2005, Rimmele 2004).

2. Mathematical model and numerical implementation

The initial temperature and density profiles are

$$T = T_0(1+\theta z), \qquad \rho = \rho_0(1+\theta z)^m, \tag{2.1}$$

with the 0 subscript defining the quantity at the top of the box ($z=0$), θ the initial temperature gradient, and m the polytropic index. Throughout we have used $T_0 = 1$, $\rho_0 = 1$, $\theta = 10$ and $m \in \{1, 1.495\}$, which gives a top layer of the solar convection zone that lies between 500 km and 6000 km beneath the visible surface. We solve the equations for fully compressible, nonlinear magnetoconvection:

$$\frac{\partial \rho}{\partial t} + \nabla\cdot(\mathbf{u}\rho) = 0 \tag{2.2}$$

$$\frac{\partial \mathbf{u}}{\partial t} + \mathbf{u}\cdot\nabla\mathbf{u} + \frac{1}{\rho}\nabla P - \theta(m+1)\hat{\mathbf{z}} - \frac{\sigma K}{\rho}\nabla\cdot\tau + \frac{\sigma\zeta_0 K^2 Q}{\rho}\mathbf{j}\times\mathbf{B} = 0 \tag{2.3}$$

$$\frac{\partial T}{\partial t} + \mathbf{u}\cdot\nabla T + (\gamma-1)T\nabla\cdot\mathbf{u} - \frac{\gamma K}{\rho}\nabla^2 T - \frac{\zeta_0 K}{\rho}|\mathbf{j}|^2 = 0 \tag{2.4}$$

$$\frac{\partial \mathbf{B}}{\partial t} - \nabla\times(\mathbf{u}\times\mathbf{B}) - \zeta_0 K\nabla^2\mathbf{B} + \nabla\psi = 0 \tag{2.5}$$

$$\frac{\partial \psi}{\partial t} + c_h^2\nabla\cdot\mathbf{B} + \frac{c_h^2}{c_p^2}\psi = 0 \tag{2.6}$$

The quantity ψ was introduced to help with divergence clearance (Dedner *et al.* 2002) and is evolved by equation (2.6). Velocity c_h is associated with the CFL condition and $c_p^2 = \alpha c_h$, where α is a chosen constant, the amplitude of which is chosen to minimize the value of $\max(\nabla \cdot \mathbf{B})$. The set of equations is evolved in a three-dimensional (3D) cylinder, so that the velocity and magnetic field are $\mathbf{u} = \mathbf{u}(r, \phi, z)$ and $\mathbf{B} = \mathbf{B}(r, \phi, z)$. We use

$$P = \rho T, \qquad \nabla \cdot \mathbf{B} = 0, \qquad \mathbf{j} = \nabla \times \mathbf{B}, \tag{2.7}$$

with the notation: τ the rate of strain tensor; γ the ratio of specific heats; σ the Prandtl number; K the dimensionless thermal conductivity; ζ_0 the magnetic diffusivity ratio at $z = 0$; Q the Chandrasekhar number. All quantities are dimensionless, with length scaling proportional to the depth of the numerical domain, time proportional to the depth divided by the sound speed at the domain top, and temperature, magnetic field, density, pressure all scaling proportional to their initial values at the domain top.

The numerical grid is a 3D wedge of a cylinder (r, ϕ, z) with depth one unit and radius Γ. The azimuthal number $M_\phi = 2\pi/\phi_{max}$ quantifies its width. The numerical model operates with $M_\phi \geqslant 4$. The top boundary conditions on the domain is as follows: the magnetic field is vertical with the temperature obeying Stefan's law. At the bottom of the domain the magnetic field is vertical and the temperature is fixed. The outside wall is slippery, perfectly conducting and thermally insulating, while the following regularity condition applies to the central axis:

$$\frac{\partial \rho}{\partial r} = u_r = u_\phi = \frac{\partial u_z}{\partial r} = B_r = B_\phi = \frac{\partial B_z}{\partial r} = \frac{\partial T}{\partial r} = 0. \tag{2.8}$$

The numerical domain is periodic in the azimuthal direction. In the numerical simulations we use a fourth-order Bulirsch-Stoer type time integration, with sixth-order compact finite differencing (Lele 1992) in the (r, z) plane and a spectral treatment azimuthally. The level of dealiasing increasing towards the central axis to maintain grid uniformity.

3. Ground state and linear azimuthal modes

The simulation is initialized with an axisymmetric, time independent ground state, which has a well defined flux tube at the central axis and two convection cells towards the outer boundary (Hurlburt & Rucklidge 2000, Botha, Rucklidge & Hurlburt 2006). This was obtained with parameter values $Q = 100$, $\sigma = 1$, $\zeta_0 = 0.2$ and $\gamma = 5/3$. This nonlinear ground state is then perturbed in the azimuthal direction. After an initial period of adjustment, linear modes appear that grow steadily until the numerical solution reaches its nonlinear state. The growth rates of the linear modes for two sets of parameters are shown in Figure 1. In order to determine the influence of the magnetic field, the calculations were repeated with the magnetic field averaged in the azimuthal direction after each time step. For the parameter set $R = 10^4$ and $m = 1$ the growth of all modes is steady, with the highest growth rates occurring for the widest wedges. Thin wedges experience damping of all perturbations. For modes when $R = 10^5$ and $m = 1.495$ the full calculation shows steady growth when $M_\phi \leqslant 6$ and oscillatory growth when $M_\phi \geqslant 8$, with the highest growth rate obtained when $M_\phi = 12$. The averaged magnetic field calculations show oscillatory growth for all modes.

The vertical velocity (r, z) contours show the form of the linear eigensolutions (Figure 2). They fill the numerical domain outside the magnetic flux tube where the convection cells are located. For steady modes (obtained when $R = 10^4$) each convection cell has a local minimum or maximum at its centre, while the shapes of the oscillating modes (when $R = 10^5$) are more fluid. The larger the local peak value, the more space it takes in the numerical domain.

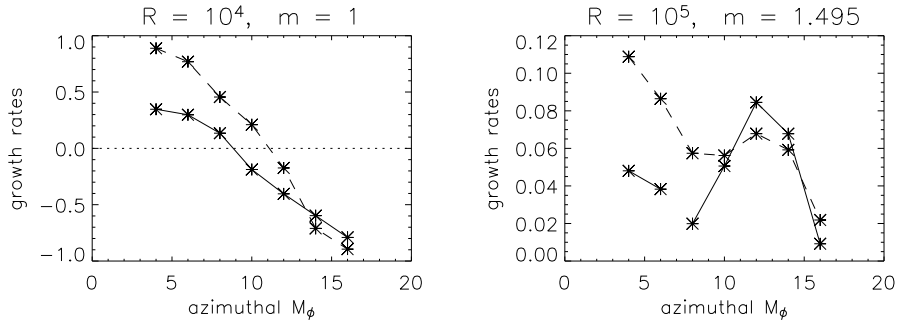

Figure 1. Linear mode growth rates obtained with two sets of parameter values. Results from the full magnetic field calculations are presented by the solid curve, while the averaged magnetic field is presented by the dashed curve. All modes show steady growth for $R = 10^4$. For $R = 10^5$ the full calculation shows steady growth for $M_\phi \leqslant 6$ and oscillatory growth for $M_\phi \geqslant 8$. All modes are oscillatory when the averaged magnetic field is used.

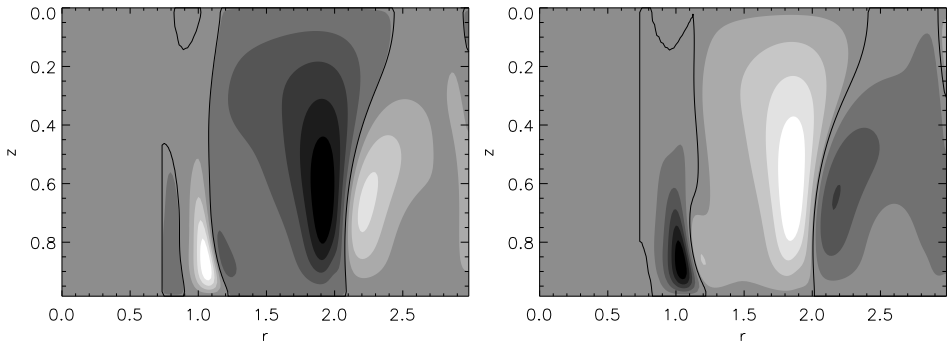

Figure 2. Contour plots of the azimuthal perturbation of u_z at a fixed azimuthal angle, obtained with $M_\phi = 10$. The oscillating mode is shown at time 55.66 (on the left) and half a period later at time 93.78 (on the right). The lighter shades are positive contours and the darker shades negative, with the black line the zero contour. The scale between contours is logarithmic. Enhanced dealiasing at the central axis (used to provide grid uniformity) set all modes to zero between $0 < r < 0.7$. The magnetic flux tube of the ground state occupies $0 < r < 1.2$.

These linear studies may throw some light on the formation of structures around pores and sunspots. They are the first results in a project that aims to simulate the formation of penumbral structures in 3D magnetoconvection numerical simulations.

Acknowledgements

GJJB was supported by PPARC through grant PPA/G/O/2002/00014.

References

Botha G.J.J., Rucklidge A.M., Hurlburt N.E. 2006, *MNRAS* 369, 1611
Dedner A., Kemm F., Kröner D., *et al.* 2002, *J. Comp. Phys.* 175, 645
Hurlburt N.E. & Rucklidge A.M. 2000, *MNRAS* 314, 793
Langhans K., Scharmer G.B., Kiselman D., *et al.* 2005, *A&A* 436, 1087
Lele S.K. 1992, *J. Comp. Phys.* 103, 16
Rimmele T.R. 2004, *ApJ* 604, 906
Sankarasubramanian K. & Rimmele T. 2003, *ApJ* 598, 689
Sobotka M., Vázquez M., Bonet J.A., *et al.* 1999, *ApJ* 511, 436